NeuroImage: Clinical 13 (2017) 297–309

Contents lists available at ScienceDirect

NeuroImage: Clinical

journal homepage: www.elsevier.com/locate/ynicl

Functional MRI vs. navigated TMS to optimize M1 seed volume delineation for DTI tractography. A prospective study in patients with brain tumours adjacent to the corticospinal tract

Carolin Weiss Lucas[a,*,1], Irada Tursunova[a,1], Volker Neuschmelting[a], Charlotte Nettekoven[a], Ana-Maria Oros-Peusquens[b], Gabriele Stoffels[b], Andrea Maria Faymonville[a], Shah N. Jon[b,e,f,g,h], Karl Josef Langen[b,e], Hannah Lockau[d], Roland Goldbrunner[a], Christian Grefkes[b,c]

[a] University of Cologne, Center of Neurosurgery, 50924 Cologne, Germany
[b] Institute of Neuroscience and Medicine, Research Centre Jülich, 52425 Jülich, Germany
[c] University of Cologne, Department of Neurology, 50924 Cologne, Germany
[d] University of Cologne, Department of Radiology, 50937 Cologne, Germany
[e] RWTH Aachen University, University Clinic Aachen, Departments of Nuclear Medicine and Neurology, 52074 Aachen, Germany
[f] Department of Electrical and Computer Systems Engineering, Monash University, Melbourne, Victoria, Australia
[g] Monash Institute of Medical Engineering, Monash University, Melbourne, Victoria, Australia
[h] Monash Biomedical Imaging, School of Psychological Sciences, Monash University, Melbourne, Victoria, Australia

ARTICLE INFO

Article history:
Received 13 October 2016
Received in revised form 18 November 2016
Accepted 19 November 2016
Available online 23 November 2016

Keywords:
nTMS
fMRI
CST
Somatotopic
Pyramidal tract
Deterministic
ROI

ABSTRACT

Background: DTI-based tractography is an increasingly important tool for planning brain surgery in patients suffering from brain tumours. However, there is an ongoing debate which tracking approaches yield the most valid results. Especially the use of functional localizer data such as navigated transcranial magnetic stimulation (nTMS) or functional magnetic resonance imaging (fMRI) seem to improve fibre tracking data in conditions where anatomical landmarks are less informative due to tumour-induced distortions of the gyral anatomy. We here compared which of the two localizer techniques yields more plausible results with respect to mapping different functional portions of the corticospinal tract (CST) in brain tumour patients.
Methods: The CSTs of 18 patients with intracranial tumours in the vicinity of the primary motor area (M1) were investigated by means of deterministic DTI. The core zone of the tumour-adjacent hand, foot and/or tongue M1 representation served as cortical regions of interest (ROIs). M1 core zones were defined by both the nTMS hotspots and the fMRI local activation maxima. In addition, for all patients, a subcortical ROI at the level of the inferior anterior pons was implemented into the tracking algorithm in order to improve the anatomical specificity of CST reconstructions. As intra-individual control, we additionally tracked the CST of the hand motor region of the unaffected, i.e., non-lesional hemisphere, again comparing fMRI and nTMS M1 seeds. The plausibility of the fMRI-ROI- vs. nTMS-ROI-based fibre trajectories was assessed by a-priori defined anatomical criteria. Moreover, the anatomical relationship of different fibre courses was compared regarding their distribution in the anterior-posterior direction as well as their location within the posterior limb of the internal capsule (PLIC).
Results: Overall, higher plausibility rates were observed for the use of nTMS- as compared to fMRI-defined cortical ROIs ($p < 0.05$) in tumour vicinity. On the non-lesional hemisphere, however, equally good plausibility rates (100%) were observed for both localizer techniques. fMRI-originated fibres generally followed a more posterior course relative to the nTMS-based tracts ($p < 0.01$) in both the lesional and non-lesional hemisphere.
Conclusion: NTMS achieved better tracking results than fMRI in conditions when the cortical tract origin (M1) was located in close vicinity to a brain tumour, probably influencing neurovascular coupling. Hence, especially in situations with altered BOLD signal physiology, nTMS seems to be the method of choice in order to identify seed regions for CST mapping in patients.

Abbreviations: APB, Abductor pollicis brevis muscle; BOLD, Blood-oxygenation-level dependent; CST, Corticospinal tract; DCS, Direct cortical stimulation; dMRI, Diffusion magnetic resonance imaging (i.e., diffusion-weighted imaging, DWI); DTI, Diffusion tensor imaging; EF, Electric field; EMG, Electromyography; FACT, Fibre assignment by continuous tracking; FA(T), Fractional anisotropy (threshold); FWE, Family-wise error; FOV, Field-of-view; fMRI, Functional magnetic resonance imaging; KPS, Karnofsky performance scale; LT, Lateral tongue muscle, anterior third; M1, Primary motor cortex; MEP, Motor-evoked potential; MFL, Minimal fibre length; MPRAGE, Magnetization prepared rapid acquisition gradient echo (T1 MR seq.); nTMS, Neuronavigated transcranial magnetic stimulation; OR, Odd's ratio; PLIC, Posterior limb of the internal capsule; PM, Plantar muscle; RMT, Resting motor threshold; ROI, Region-of-interest; SD, Standard deviation; SE, Standard error; X-sq, X-squared (Pearson's chi-square test); p_{xsq}, *p*-value according to Pearson's chi-square test.

* Corresponding author at: Klinik für Allgemeine Neurochirurgie, Uniklinik Köln, Bettenhaus Eb. 8. Kerpener Str. 62., 50931 Cologne, Germany.
E-mail address: carolin.weiss@uk-koeln.de (C. Weiss Lucas).
[1] Both authors contributed equally to the manuscript (shared first authorship).

http://dx.doi.org/10.1016/j.nicl.2016.11.022

1. Introduction

Even small white matter tract lesions, especially when affecting the structural integrity of the corticospinal tract (CST), can lead to severe functional damage such as hemiparesis. Therefore, the preservation of the structural integrity of important white matter tracts is of great interest in the treatment of neurological diseases. The introduction of diffusion-weighted magnetic resonance imaging (dMRI) for non-invasive visualization of white matter tracts has not only widened the view on structural connectivity in general but also extended the options for treatment planning (Strick and Preston, 1983; Petrides and Pandya, 1984; Le Bihan et al., 2001; Barone et al., 2014). Techniques such as diffusion-tensor imaging (DTI) enable tractography of critical neural tracts like the CST, and have been successfully applied to improve the function-preserving resection of brain tumours (Nimsky et al., 2004, 2007; Wu et al., 2007; Svolos et al., 2014). To reconstruct the pyramidal tract for clinical applications, a deterministic approach based on multiple regions-of-interest (ROI) including the cortical primary motor representation (M1) as a starting (seeding) point for tractography represents the most common algorithm (Mori and van Zijl, 2002). The correct placement of the cortical seeding ROI represents a critical factor for obtaining valid tractography results in such a multiple-ROI approach. There is increasing evidence suggesting that the validity of anatomical landmarks has been widely overestimated (Zilles et al., 1997): Even the localization of the M1 hand representation – which is typically found at the "hand knob" formation of the precentral gyrus (Yousry et al., 1997) - seems to vary significantly between healthy subjects (Diekhoff et al., 2011; Ahdab et al., 2016). Thus, several functional localizer techniques such as functional MRI (fMRI) (Conturo et al., 1999; Guye et al., 2003; Parmar et al., 2004; Staempfli et al., 2008), magnetic encephalography/magnetic source imaging (Gaetz et al., 2010) and, more recently, navigated transcranial magnetic stimulation (nTMS) (Frey et al., 2012; Krieg et al., 2012) have been used in order to optimize and standardize the DTI tractography of the CST. We recently showed that the use of a subcortical ROI placed in the anterior inferior pontine region is advantageous as compared to the posterior limb of the internal capsule (PLIC) using nTMS to delineate the cortical M1-ROI (Weiss et al., 2015). However, there is still little evidence regarding the question of which functional localizer technique is most suited for CST tracking in brain tumour patients. fMRI is prone to tumour-induced alterations of the haemodynamic response and/or neurovascular coupling and, thus, blood-oxygenation-level dependent (BOLD) activity in the surrounding of tumours may be misinterpreted (Lehéricy et al., 2000; Wengenroth et al., 2011; Wehner, 2013). By contrast, nTMS has different limitations such as in patients with severe motor deficits resulting in reduced or abolished motor-evoked potentials (MEPs). Furthermore, fMRI tasks require active movement initiation by the subject and thus compliance, whereas nTMS results can e.g. be altered by medication (affecting the resting motor threshold) and reduced tolerability due to direct nerve stimulation when stimulating over the frontolateral region, i.e. the face representation (Weiss et al., 2013).

The objective of this study, therefore, was to compare fMRI vs. nTMS for defining the seeding ROIs for somatotopic tractography of the hand-, foot- and face-related CST.

We hypothesized that fMRI activation maxima may be less reliable in case of close vicinity to the tumour due to tumour-induced alterations of haemodynamic effects in cortical ROIs and unfavourable signal-to-noise ratio which in turn would lead to less plausible tractography results.

On the other hand, nTMS was expected to show more variable results for the foot and the tongue representations which are usually more difficult to map and have shown less reliable mapping results (Weiss et al., 2013). In addition, we reasoned that better plausibility results were associated with higher fractional anisotropy (FA) values which serve as observer-independent parameters and represent diffusion metrics corresponding to the directionality of diffusivity and thus to the fibre integrity.

2. Material and methods

2.1. Patients

Thirty-two patients (21 male, mean age 57 ± 14 yrs) scheduled for the resection of intracranial tumours adjacent to or involving the precentral gyrus – representing M1 – and/or the CST were prospectively screened between 2012 and 2013. All patients had a surgical indication for tumour removal and, due to the tumour location, for non-invasive preoperative as well as (invasive) intraoperative mapping of the operation field. Only patients showing functional intact peri-lesional tissue (in a distance of <2 cm from the tumour margin) as verified by intraoperative DCS were included in the study ($N = 18/32$; 10 male; mean age 50 ± 13 yrs).

All patients included in the study were (i) eligible for MRI, (ii) in a rather good clinical state as indicated by the Karnofsky performance scale (KPS) > 70% (Karnofsky and Burchenal, 1949) and (iii) able to follow the experimental protocol. By contrast, patients were excluded in case of severe renal failure (glomerular filtration rate < 30 ml/min) due to contraindication with respect to the administration of gadolinium-contrast agent or if they suffered from uncontrolled epilepsy (generalized seizure within 48 h prior to nTMS, insufficient dosage of anticonvulsive drugs in case of previous seizures). Please note that like in other single pulse nTMS studies with brain tumour patients (Tarapore et al., 2016b), epilepsy was not considered as a general exclusion criteria as long as all patients were under effective anticonvulsive treatment. Since the risk of inducing a seizure was considered very low in the given patient selection, it was clearly outweighed by the benefit of gathering information about eloquent cortex in order to prevent operation-induced motor disability. In fact, none of the patients suffered from any epileptic event during or after participating at the present study.

Further exclusion criteria were: age (<18 yrs), severe migraine/headache, claustrophobia, pregnancy, metal/electric implants, severe psychological disorder and severe cognitive deficits (severe receptive/global aphasia, neglect). Moreover, intake of medication affecting ionic channels was avoided, as far as possible, in order to minimize extrinsic factors modulating the motor cortex excitability. Written informed consent was obtained from all patients. All patients were treated in the Department of Neurosurgery, Cologne University Hospital/Germany. The study was approved by the local ethics committee of the Medical Faculty of the University of Cologne.

2.2. Study design

All patients were investigated by fMRI and nTMS prior to surgery. Of note, all somatotopic M1 representations in close relationship to the tumour as well as the contralateral M1 hand representation were investigated by separate fMRI tasks/nTMS mappings. Moreover, patients were investigated by fMRI-, nTMS- and DTI-based tractography of the CST prior to surgery. Intraoperatively, DCS was performed as reference standard to prove the functionality of peri-tumoral cortical tissue. NTMS- and fMRI-derived somatotopic fibre tracts were then compared regarding the plausibility of the fibre course, the fibre location when passing

the internal capsule as well as diffusivity metrics (fractional anisotropy) with regard to the lesional vs. the contralateral hemisphere (see Data analysis).

2.3. Structural MRI acquisition

All measurements were performed on a 3 T MR scanner (MAGNETOM Trio, Siemens Healthcare, Erlangen, Germany) equipped with gradients of maximum strength of 40 mT/m per axis. A birdcage coil was used for radiofrequency transmission and an 8-element receiver coil for signal detection. Data quality was examined at the beginning of the measurement protocol by acquiring a single b = 0 diffusion-weighted magnetic resonance imaging (dMRI) scan – that is, no diffusion weighting – and inspecting it for artefacts. The detailed diffusion-weighted magnetic resonance imaging (dMRI) acquisition parameters have been previously reported by our group (Weiss et al., 2015). The MR protocol included the following sequences: MP-RAGE (T1-weighted) before and after gadolinium (Gd) contrast agent, SPACE (T2-weighted), FLAIR and BOLD-fMRI. The total acquisition time for the MR measurements was <1 h (including 7:20 min. diffusion-weighted magnetic resonance imaging (dMRI) measurement).

2.4. fMRI

2.4.1. Data acquisition

The fMRI task was designed to elicit activations associated with movements of the same muscles as used for MEP recordings (nTMS) and was identical to the task used in our previous work (cf. Weiss et al., 2013). Subjects were continuously monitored during task performance in the scanner by an investigator standing next to the scanner bed. Motor performance in terms of movement frequency was very stable across sessions in each subject due to the relative simplicity of the tasks.

We used a gradient-echo planar imaging (EPI) sequence sensitive to detect blood-oxygenation-level dependent changes in tissue contrast using established imaging parameters (cf. Weiss et al., 2013). In fMRI, the signal-to-noise ratio, and hence stability of the data, are influenced by the acquisition plane (Gustard et al., 2001). Here, slice orientation was axial, slightly tilted backwards so that the orientation of the slices was approximately perpendicular to the course of the central sulcus.

2.4.2. fMRI preprocessing

The MRI volumes were processed using the Statistical Parametric Mapping software package (SPM 8; Wellcome Department of Imaging Neuroscience, London, UK, http://www.fil.ion.ucl.ac.uk) implemented in Matlab (version 2011, The MathWorks Inc., MA, USA). The first three images were excluded from further analyses ("dummy images"). The remaining EPI volumes were realigned to the first volume by affine registration using a two-pass procedure. The realigned EPIs were then co-registered with the corresponding high resolution T1 volume. Due to the tumour-induced changes in cortical and subcortical anatomy, group comparisons were not considered appropriate. EPI volumes were spatially smoothed using an isotropic Gaussian kernel of 8 mm full-width-at-half-maximum (FWHM).

2.4.3. fMRI statistics

The experimental conditions were modelled using boxcar stimulus functions convolved with a canonical haemodynamic response function. The time series in each voxel were high-pass filtered at 1/128 Hz. A one-way General Linear Model (GLM) was applied for identification of significantly activated voxels. Head movement estimates were used as confound regressors. For single subject analyses, a threshold of $p < 0.05$, family-wise error (FWE) corrected was used to identify significant voxels. In case of none significant voxel, statistical thresholds were lowered to uncorrected values which was the case in 17% of the sessions. The non-lesional hemisphere was used as an intra-individual control (since the precentral gyrus was not always easy to determine in the vicinity of brain tumours with mass effect). The obtained local activation maxima were labelled using MRIcron, exported as analyze-format image sets and integrated into the neuronavigation software (Brainlab iPlan 3.0.0, Heimstetten, Germany). Potential errors resulting from image export and fusion were checked by comparing the respective peak voxel coordinates derived from the fMRI statistics and the final coordinate taken from the iPlan voxel space.

2.5. nTMS

2.5.1. Data acquisition

NTMS was conducted using the NBS system (version 4.2, Nexstim Ltd., Helsinki, Finland) and a figure-of-eight-shaped stimulation coil. Along with preparations and co-registration, as reported in more detail in our previous works (cf. Weiss et al., 2013, 2015), surface electrodes (Ambu Neuroline, Bad Nauheim, Germany) were mounted above the abductor pollicis brevis muscle (APB), the plantar muscle (PM) and the anterior lateral tongue muscles (LT), whenever clinically meaningful, i.e., whenever the respective body part representation or associated CST fibres were adjacent to the tumour, for motor-evoked potentials (MEPs) recordings. To avoid false-positive registration of nTMS-induced MEPs, the following latency ranges were applied for the respective groups of muscles: 17–30 ms for APB, 31–60 ms for PM, and 9–16 ms for LT (Weiss et al., 2012, 2013, 2015; Rödel et al., 1999, 2001, 2003; Saisanen et al., 2008). As an intra-individual control, data were additionally acquired from the APB of the unaffected side.

Stimulation intensity was adjusted to 110% of the resting motor threshold (RMT) of the respective muscle, which was determined at the estimated "hot-spot" of the respective body part representation. The anatomical position of the hot-spot was established by performing a coarse mapping around the anatomical landmarks of the respective motor cortex representation area (Penfield and Rasmussen, 1950; Weiss et al., 2013): (i) the "hand knob formation" (Yousry et al., 1997) for hand mapping, (ii) the cortex close to the interhemispheric fissure for foot representation mapping, and (iii) the frontal operculum for the lips and tongue area. The hot-spot was defined as the cortical stimulation site at which coil positioning, orientation and tilt yielded the highest MEP amplitude. The RMT was defined as the minimum stimulus intensity capable of inducing MEPs > 50 μV peak-to-peak amplitude in at least 5 out of 10 consecutive trials in the estimated hot-spot of the relaxed muscle (Rossini et al., 1994; Julkunen et al., 2009). The coil orientation was kept stable (according to its orientation at the hot-spot) during the whole mapping procedure of a given body part representation and was perpendicular to the respective sulcus (Janssen et al., 2015; Raffin et al., 2015). For mapping of the tongue area, some nTMS sessions required voluntary pre-innervation to reduce excitability thresholds and thus to prevent direct nerve stimulation causing discomfort and short-latency potentials. For each muscle representation, 120–200 pulses (depending on the size of the respective representations and subject compliance) were applied using a stimulation grid (space between nodes: 5 mm, independent from coil orientation) projected onto the reconstructed brain surface during the exam. The application of two to three pulses per grid square unit was attempted in all cases. The outer margin of each functional map was determined by two adjacent negative MEP responses (i.e., MEP amplitude <50 μV; Weiss et al., 2013, 2015).

2.5.2. Data processing

At the end of the nTMS mapping, all positive EMG responses underwent manual selection with regard to the effects of potential involuntary pre-innervation and to eliminate false-positive results. Thereafter, the stimulus evoking the highest MEP response was selected and its cortical representation, i.e. the hot-spot, was exported in a series of binarized DICOM images for each body part representation, separately. DICOM export was performed at a chosen peeling depth of

approximately 20 mm (default), according to the level at which the cortical grey matter (but not white matter) was displayed in the 3D peeling view (i.e., at the "top" of the white matter part of the gyrus). The peeling level was adjusted in the *z*-axis of the maximum electric field (EF) strength according to the coil position (Ilmoniemi et al., 1999) as provided by the EF-calculation algorithm integrated in the software of the TMS machine (Ruohonen and Karhu, 2010) and was 17.3 ± 3.1 mm (skin-target-distances) on the lesional hemisphere. The site of the maximum TMS effect, however, can only be roughly estimated by such algorithms since (i) an effect on more superficial (inter-)neurons, as compared to the peeling level, has to be considered due to the EF-characteristics and the decay of EF strength with increasing distance from the coil (Salinas et al., 2007) and (ii) neurophysiological effects do not only depend on the EF strength but also on the orientation of axons respective to the EF-orientation and the, eventually brain-state-dependent, excitability of neuronal tissue.

2.6. DCS

DCS mapping was performed in clinical routine to identify functionally intact cortex during operation. Depending on tumour location and size of skull removal, part of M1 could be mapped by the surgeon using DCS. We used the DCS data to verify the proximity between intact functional tissue (i.e., somatotopic M1 representation) and the tumour. We here briefly describe the DCS procedure:

2.6.1. General anaesthesia

Surgery was performed under general anaesthesia following standard clinical protocols avoiding relaxans (except for intubation) and including a total intravenous analgetic regime (Scheufler and Zentner, 2002).

2.6.2. DCS procedure

Standard EMG needles (Ambu® Neuroline) were placed into the muscles corresponding to the nTMS/fMRI protocol described above (APB, PM, LT) and fixed by additional tape/gaze. After craniotomy and durotomy, the assumed hot-spots of the exposed M1 areas were addressed one-by-one using the navigation system and the integrated functional data (Brainlab Vector Vision/iPlan). A monopolar probe with a spherical tip was referenced as a navigated "tool" using the navigation system and then placed at the respective hot-spots/local activation maxima for separate threshold determination. To evoke the MEPs, anodal rectangular pulses were applied (500 Hz, 500 μs; Szelényi et al., 2011). For threshold determination, the core area of the functional nTMS map was addressed first. At this cortical site, stimulation intensity was systematically increased starting from 10 mA until a MEP > 50 μV could be evoked in >50% (3 out of 5) of the stimulation trains (max. 25 mA; stimulator: Viasys ENDEAVOR CR). Thereafter, the surrounding of the core zone was stimulated at suprathreshold stimulation intensities (motor threshold of the respective somatotopic representation + 1 mA, max. 25 mA) and the threshold was adjusted in case of stronger MEP responses (i.e., higher amplitude) at distinct cortical sites. In particular, the margin of the functional cortical tissue facing the tumour was outlined in order to assess the minimal distance from the tumour. As described above, only such patients for which a distance of 2 cm or less between the tumour (margins projected on cortex level using the intraoperative neuronavigation system iPlan) and the functional tissue was confirmed by DCS were included in the analysis. However, mapping was limited by reduced cortical excitability (depending on the anaesthesiological management), the subarachnoidal space and superficial vessels such as bridging veins, especially when stimulating the foot representation, limited exposure of areas (size of craniotomy), significant brain shift after durotomy ($N = 2$) and, rarely, technical problems such as needle dislocation or data loss due to software shutdown ($N = 1$).

Out of thirty-two screened patients with intracranial tumours, $n = 18$ were included in the study for which DCS was well-feasible and had proven the close vicinity (<2 cm) of the tumour to the margin of at least one somatotopic M1 representation.

2.7. Tractography

The results of the functional localizer experiments, i.e., the binarized DICOM series displaying the cortical representation of the respective nTMS hot-spot and the fMRI local activation maxima as well as the anatomical MRI and eddy-current-corrected DTI sequences were imported into the tracking software (Brainlab iPlan 3.0.0, Heimstetten, Germany) prior to surgery. Tracking was performed using a deterministic fibre tracking algorithm which integrates voxel-wise diffusion properties for fibre assignment by continuous tracking (FACT) (Mori et al., 2002) and a multiple-ROI approach as described below. Post hoc, those tracts for which motor-eloquent localization was confirmed by DCS intraoperatively were selected for further analysis. Moreover, for each of those cases, the contralateral hand-related tract was also included (as individual reference under non-lesional tissue conditions). Thus, the number of somatotopic and localizer-technique-specific tracts included in the study varied between subjects, depending on the tumour localization and the DCS results, and ranged from four to eight (N = 1 contralateral and N = 1–3 ipsilesional somatotopic tracts, each "dual" tract, originating from the fMRI- vs. the nTMS-M1).

2.7.1. Definition of seeding ROIs: cortical M1 ROIs

The nTMS- and fMRI-derived DICOM series displaying the hot-spot/local activation maxima were co-registered with the anatomical MR image which had been used for the nTMS before. Thereafter, the respective sequence was co-registered with further anatomical sequences (T2, FLAIR) and the b = 0 dataset of the DTI time-series. Fusion accuracy with nTMS data was checked by comparing the respective coordinates provided by visualization software (iPlan) with the raw data (coordinates). The coordinates corresponded to the site of maximum EF (see nTMS; Data processing) and were located 3 ± 1 mm below the surface of the closest cortex. The fusion-associated mismatch was <2 mm in all subjects. Hot-spots and local activation maxima were labelled as ROIs and enlarged by 2–3 mm, according to the estimated registration and fusion mismatch, so that the volumes of the resulting spherical cortical ROIs representing the M1 hots-pots were standardized to a total volume of 0.9 ± 0.1 cm^3 (Weiss et al., 2015) (Fig. 1).

2.7.2. Subcortical ROIs

A cubic box was inserted in the region of the anterior inferior pontine level (Seo and Jang, 2013) which we recently showed to be favourable compared to the posterior limb of the internal capsule (Weiss et al., 2015). The standard location to insert the cubic ROI (with a craniocaudal extension of 7.5 ± 1 mm) within the field-of-view of the diffusion-weighted magnetic resonance imaging (dMRI) (i) was caudally from the upper and middle cerebellar peduncle, centred over the cross-sectional level of the maximal a.-p. extension of fourth ventricle and the cerebellar nodule in the sagittal view and (ii) comprised the anterior two thirds of the pons, measured from the rostral margin of the fourth ventricle in the cross-sectional view (mean ROI volume: 3.6 ± 0.7 cm^3) (Fig. 2). Of note, one (same) cubic pontine ROI was created per subject and served as second ROI for all tractographies, regardless of the somatotopic affiliation and the functional localizer technique used to delineate the cortical ROI.

2.7.3. Fibre tracking parameters

All fibres were calculated originating from the cortical hot-spot/local activation maxima ROIs, with the additional pontine ROI box. Vector step length was 1.6 mm and the angular threshold was 30°. The minimal fibre track length (MFL) was not pre-set and, thus, set at the minimum of MFL = 1 allowed by the software (Weiss et al., 2015). To compute the

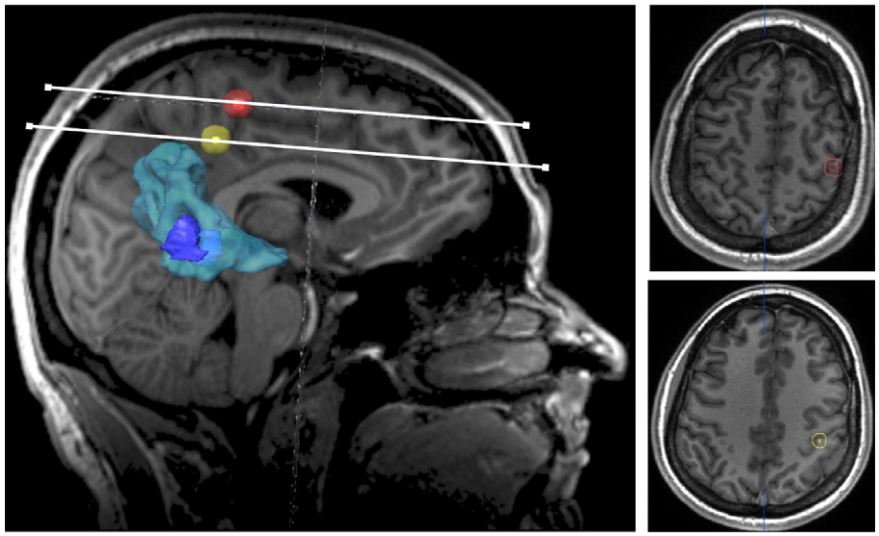

Fig. 1. Cortical regions of interest representing the M1 core area. For each functional localizer method, i.e., nTMS, fMRI and DCS, the core area (hot-spot/local activation maxima) was separately determined, integrated into the neuronavigation software and enlarged to a spherical volume of 0.9 cm^3 ($\pm$0.1) (here: hand representation). Here, a patient with postcentral glioma (contrast-enhancing tumour volume outlined in dark blue) with strong perifocal oedema (outlined in light blue) is shown. The hot-spot of the M1 hand representation depicted by nTMS prior to surgery (red) was very close to the DCS hot-spot (orange) whereas the fMRI local activation maximum (yellow) was located slightly posteriorly and deeper within the white matter.

fractional anisotropy threshold (FAT), the FA value was gradually increased or decreased until the highest FA value was identified which resulted in at least one reconstructed fibre. This value was defined as 100% FAT and the resulting fibres were used for the analyses (Weiss et al., 2015) to allow for maximal distinction of the different fibre courses (Fig. 3). This approach should not be taken in contrast but complementary to the suggestion of other authors who proposed to use lower FA values of 75% FAT (Frey et al., 2012) with regard to increased sensitivity and thus safety in brain tumour surgery.

2.8. Data analysis

2.8.1. Plausibility ratings

All fibre tracts (contralesional hand, ipsilesional: hand, foot, tongue; based on nTMS vs. fMRI seeding ROIs), were analyzed separately. The analysis was performed using the neuronavigation software (iPlan) which enables the observer to switch between cross-sectional views in any plane (axial, sagittal, coronal) as well as labelling of ROIs and determination of localizations in 3D coordinates. Plausibility ratings were performed in a dichotomic manner (i.e., yes/no) by two investigators experienced in the anatomical allocation of fibre tracts, applying the decision-making rules previously published by our group (cf. Weiss et al., 2015).

2.8.2. Influence of cortical ROI positioning method on fibre course plausibility

McNemar's chi-square test (McNemar, 1947) for paired binary data was used to test for differences in plausibility ratings between nTMS- vs. fMRI-based tractography conditions (within the same group of patients and with the same observer). The level of confidence was defined at 95% ($p < 0.05$).

2.8.3. Fibre-associated distance metrics

The distances between each reconstructed fibre and the mid-line was measured in the axial plane at the level of (i) the maximum tumour extent, (ii) the interventricular foramen of Monro and (iii) the tentorial notch. Moreover, the distances between the pairs of localizer-derived somatotopic tracts (i.e., fMRI-nTMS and, whenever obtained, fMRI-DCS and nTMS-DCS) were measured in the same axial planes (i–iii) using the neuronavigation software (iPlan). To test for differences between the means of localizer-specific metrics, Student's *t*-test for paired samples was applied, and corrected for multiple comparisons if

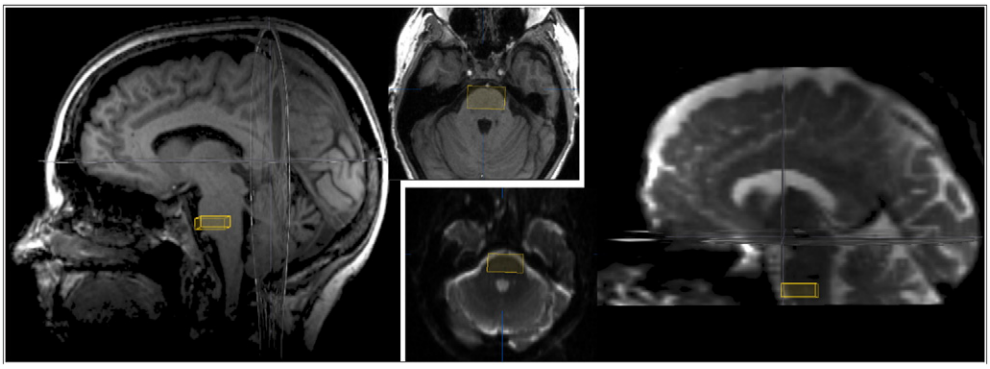

Fig. 2. Placement of the cubic subcortical ROI in the anterior inferior pontine region. According to our previous study (Weiss et al., 2015) a second subcortical ROI box (in addition to the functional cortical ROI) was set in the anterior inferior pontine region in order to apply a deterministic multiple-ROI tractography approach (Mori et al., 2002). To control for the field-of-view and artefacts in the DTI data set, the ROI placement was based on both anatomical T1 (left) and DTI series (B0 sequence; right).

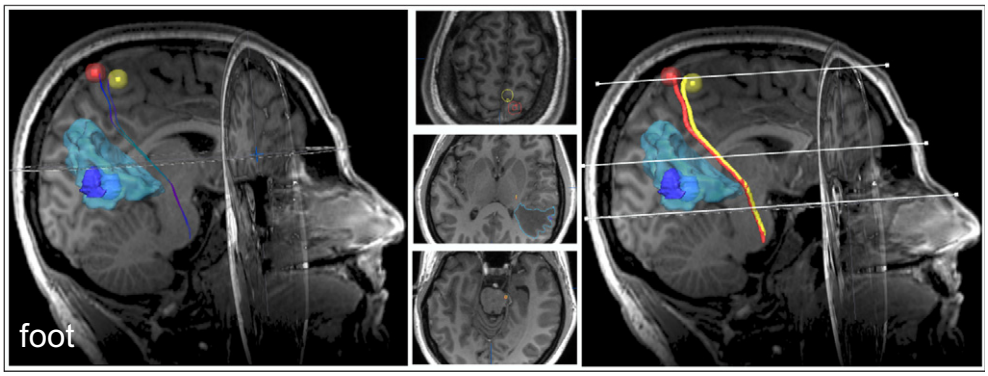

Fig. 3. Functional-localizer-derived somatotopic DTI-tractography. A pair of somatotopic corticospinal tracts originating from the cortical functional core representation of the as defined by either fMRI (yellow) or nTMS (red), both rated plausible tracts. Examples for mixed plausible/non-plausible tractography results with somatotopic hand/face affiliation are provided in the Supplementary material (Supplementary Figs. S1 and S2).

appropriate using the false discovery rate (FDR) approach (Benjamini and Hochberg, 1995; Glickman et al., 2014).

2.8.4. Fibre course within the internal capsule

According to anatomical knowledge (Verstynen et al., 2011; Pan et al., 2012; Zolal et al., 2013), the posterior limb of the internal capsule (PLIC) was identified at the level of the interventricular foramen of Monro, and segmented into three parts: (i) genu, (ii) middle PLIC and (iii) posterior PLIC (Fig. 4). Each reconstructed fibre was assigned to one of these locations (i–iii) or to the additional category "outside" which consecutively led to the judgement "non-plausible tract" (for detailed rating criteria, cf. Weiss et al., 2015). Moreover, the relationship of fMRI- and nTMS-derived somatotopic fibres in the anterior-posterior dimension was assessed on the same level in axial view, Accordingly, fMRI-derived fibres were classified "anteriorly", "posteriorly" or not distinguishable ("same") from nTMS-derived fibres for each somatotopic tract.

2.8.5. Correlation between tractography parameters and plausibility

FA values have a significant impact on fibre course plausibility. Since the influence of the minimal fibre lengths seems to represent only an epiphenomenon of the FAT impact (Weiss et al., 2015), we here focused the data analysis on the FAT. Pairwise comparisons between the FATs of different somatotopic or localizer-specific fibres were calculated using the Student's *t*-test (FDR-corrected in case of more than one comparison). Correlations between continuous variables such as the FAT and the dichotomous outcome variable, i.e., the plausibility of the CST fibre course, were calculated using Pearson's product moment (point-biserial correlation).

The statistical analyses were performed using SPSS (PASW Statistics 18.0, SPSS Inc., Chicago, IL, USA) and the R software package (version 3.0.2; R Core Team 2013; RStudio; http://www.R-project.org/).

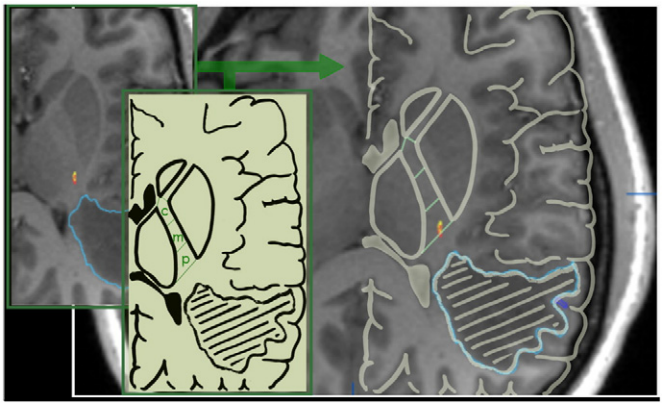

Fig. 4. Segmentation of the PLIC: The PLIC was segmented into three parts of equal length: the most rostral/central (c) segment of which included the genu; the other two parts were treated as the middle (m) and posterior (p) segment. Each fibre tract (yellow/red) was assigned to one of the segments, according to the location of its major part in the axial cross-sectional view on the level of the interventricular foramen of Monro. In this example, showing somatotopic fibres originating from the cortical M1 hot-spot/local activation maximum of the hand, both fMRI- (yellow) and nTMS- (red) derived fibre tracts were located in the posterior section of the PLIC.

3. Results

3.1. Patients and descriptive analysis

The tumour entities consisted mostly of primary brain tumours ($n = 11$) (Table 1). According the CE-T1 scans, tumours were mostly located in the precentral region (56%), as compared to 39% postcentral tumours. One tumour was located in the lateral central region and involved also the temporal lobe.

All patients were still in a rather good clinical state as indicated by the KPS (90 ± SD 11%). Almost half (44%) of the patients were admitted with a mild to moderate motor deficit. The patient cohort included eleven patients with known epilepsy (all medically treated, 55% with levetiracetame). In none of those patients, seizures were induced by the administration of single-pulse nTMS.

Half of the patients (50%) were under steroid medication at the time of nTMS. Furthermore, patients routinely received a low dose of dexamethason at the beginning of surgery. Administration of steroids may not only affect the cortical excitability through membrane stabilization effects and, thus, influence the feasibility of nTMS and DCS but also alter MRI signals and particularly diffusivity metrics. However, this confound was unavoidable since most patients had already been put under anti-oedema treatment before hospitalization and for clinical reasons (better treatment effects regarding neurological deficits and

Table 1
Distribution of tumour entities within trial subjects. The histological analysis of most recruited patients revealed high-grade gliomas ($n = 10$) and carcinoma metastases ($n = 4$).

Histopathological diagnosis	*N*
Gliomas	11
Glioblastomas	5
Astrocytomas WHO III°	5
Oligoastrocytoma WHO II°	1
Others	7
Carcinoma metastases	4
Meningiomas	2
B-cell-lymphoma	1

intracranial pressure in cases of tumours with mass effect due to large perifocal oedema).

No severe adverse effects were reported for nTMS or fMRI, 6% of the patients complained of transient headache (lasting for <24 h) after nTMS. However, the subjective level of distress was ranked higher for fMRI as compared to nTMS by 92% of the patients. Being asked for the reason, patients usually reported the duration of immobilisation and narrowness of the scanner/the head coil, respectively.

3.2. Plausibility analysis

Following DTI preprocessing, nTMS- vs. fMRI-seed-originated tracts were reconstructed for each DCS-confirmed body part connecting the cortical ROI volume to the subcortical ROI box in the anterior inferior pontine region.

3.2.1. Influence of the somatotopic assignment on fibre course plausibility

As a common finding for both nTMS and fMRI (serving as functional localizer to determine the cortical M1 ROI), fibre tracts computed for the contralesional hemisphere (origin: M1 hand) showed best plausibility results (both nTMS and fMRI: 100%) (Fig. 5). Regarding the somatotopic tracts originating from the different ipsilesional M1 representations, results varied depending on the localizer technique: NTMS provided best plausibility results for the hand-related CST (93%). In contrast, the fMRI-derived tracts originating from the ipsilesional M1 hand representation seed deviated more often from the expected course (example: Supplementary Fig. S1). Amongst different somatotopic fMRI-derived tracts, best results were obtained for those which originated from the tongue area (80%; Fig. 5). Similar results were obtained for the foot-associated fibres using the different localizer techniques (Figs. 3 and 5). In cases in which plausibility results differed between fMRI- and nTMS-derived fibres of the same subject and somatotopic affiliation, usually the fMRI- but not the nTMS-originated tracts deviated from the expected course ($N = 7$ cases: $N = 4$ hand, $N = 2$ foot, $N = 1$ tongue; example: Fig. S1). However, the opposite was also observed in one case (tongue; example: Fig. S2).

3.2.2. Comparison of ROI localization techniques

Overall, higher plausibility rates were observed for the use of nTMS- as compared to fMRI-defined cortical ROIs (nTMS: 88% vs. fMRI: 70%; $\chi^2_{McNemar} = 4.5$ [0.003–0.527], $p_{McNemar} = 0.034$). Comparing distinct somatotopic tracts, a similar difference was observed for the hand-CST (nTMS: 93% vs. fMRI: 67%; $\chi^2_{McNemar} = 4$ [0–0.602], $p_{McNemar} = 0.046$). By contrast, there was no statistical difference regarding the plausibility rates of foot- and face-related somatotopic tracts. Moreover, both localizer methods, fMRI and nTMS led to equally excellent plausibility results (100%) for reconstruction of the hand-related CST of the non-lesional hemisphere (for descriptive data, see Fig. 5).

3.3. Course of the CST

The course of the reconstructed fibres was described with regard to the distance from the midline, the distance between fMRI- vs. nTMS-originated fibres belonging to the same somatotopic subset, their position to each other in the anterior-posterior direction and their location within the PLIC.

3.3.1. Distance of fibres from the midline

The distances of each fibre from the mid-line in the axial plane were in the range of 23 ± 5 mm at the level of Monro's foramen and in the range of 10 ± 4 mm at the level of the tentorial notch (independent from functional localizer technique and somatotopic subset).

3.3.2. Distance and spatial relationship between fibres

The average distance between the nTMS- and fMRI-derived fibres varied amongst the three cross-sectional levels (maximal tumour extent: 6 ± 9 mm; interventricular foramen of Monro: 5 ± 10 mm; tentorial notch: 3 ± 9 mm). Throughout the deviated courses, a

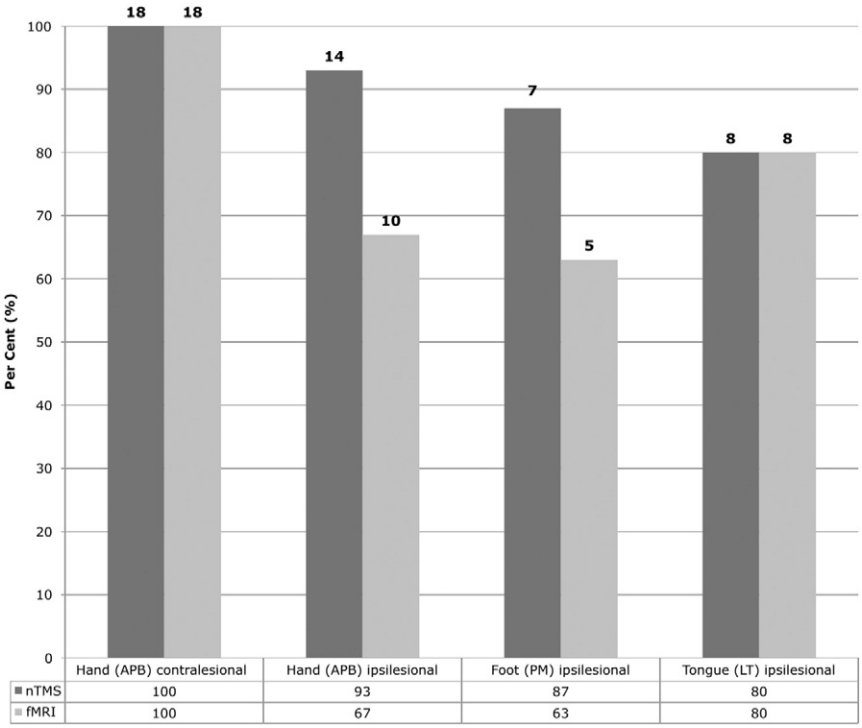

Fig. 5. Plausibility rates of somatotopic CST courses. The bar plot displays the plausibility rates (y: count of plausible tracts in % of total) and absolute numbers regarding the course of the somatotopic CST. The distinct somatotopic core ROIs within the primary motor cortex (columns) served as origins for the tracking algorithm and were determined by either nTMS (darker grey) or fMRI (light grey).

generally more posterior course of the fMRI-derived in relation to the nTMS-originated fibres was observed ($p_{XSq} < 0.01$) (Table 2).

3.3.3. Fibre course within the PLIC

According to anatomical considerations, fibres originating from M1 of the foot passed mainly through the posterior segment of the PLIC (Figs. 4 and 6) whereas hand- and face-related fibres were predominantly located in the middle segment (Fig. 6AC). Interestingly, no fMRI-derived fibres passed through the central segment/genu of the PLIC (Fig. 6).

3.4. Fractional anisotropy

There was no significant difference between the FAT values of nTMS- and fMRI-derived fibres (mean of all fibres for both: 0.22 ± 0.10). Regardless of the functional localizer technique, the highest mean FATs, as a measure of fibre integrity, were found for the fibres originating from the non-lesional hand representation (nTMS 0.28 ± 0.07/fMRI 0.29 ± 0.08) and least FATs for tongue-related tracts (nTMS 0.12 ± 0.09/fMRI 0.12 ± 0.06). The FAT values of the ipsilesional hand- and foot-related CST were in the range of 0.18–0.22 (hand: nTMS 0.22 ± 0.09; fMRI 0.19 ± 0.09; foot: nTMS 0.22 ± 0.08; fMRI 0.18 ± 0.09).

3.4.1. Correlation between FA values related to different functional localizer techniques

A high correlation was observed between the FATs of CST originating from nTMS- and fMRI-ROIs (nTMS ~ fMRI: $p < 0.0001$; CI: 0.42–0.66). With regard to the different somatotopic tracts, significant correlations were found between nTMS- and fMRI-derived FATs associated with the non-lesional (nTMS ~ fMRI [NL-hand]: $p < 0.005$; CI: 0.25–0.75) and with the lesional hand representation (nTMS ~ fMRI [L-hand]: $p < 0.01$; CI: 0.14–0.70) but not with the foot- or the tongue-related tracts.

3.4.2. Influence of FA thresholds on fibre course plausibility

For all functional localizer methods (i.e., nTMS, fMRI, DCS), a significant correlation between the FAT and the fibre course plausibility was observed (Pearson product moment correlation: nTMS: $p < 0.0001$; fMRI: $p < 0.001$; DCS: $p < 0.05$). Analyzed by somatotopic data subsets, this correlation was confirmed for all nTMS-groups (hand: $p < 0.01$, foot: $p < 0.1$, tongue: $p < 0.01$; FDR-corrected). Regarding fMRI-based tracts, only the FATs of hand-related fibres showed a significant correlation with the plausibility of the fibre course ($p < 0.01$; FDR-corrected).

4. Discussion

Both functional localizer techniques, fMRI and nTMS, were able to achieve plausible CST tractography results for the unaffected hemisphere (100% plausibility rate). By contrast, whenever the cortical seed region (M1 core voxel) was located close to the tumour, the use of nTMS to determine the seed voxel led to more plausible tractography results as compared to fMRI ($p < 0.05$), especially for the somatotopic hand-related tracts. In general, the nTMS-seed-based CSTs followed a more rostral course as compared to those fibres which originated from the fMRI-seed ($p < 0.01$).

4.1. General considerations

Over the past years, tractography-guidance has made its way to becoming a popular clinical tool to delineate important white matter tracts, due to good clinical results (Wu et al., 2007) and several proofs of convergence between the preoperative DTI-tractography and (i) intraoperative direct subcortical stimulation (DsCS) (Prabhu et al., 2011; Zhu et al., 2012; Ohue et al., 2012; Vassal et al., 2013) as well as (ii) MEP recordings from deep brain stimulation (DBS) electrodes (Forster et al., 2015). There is increasing evidence that two-tensor streamline techniques (Qazi et al., 2009), non-tensor approaches (Auriat et al., 2015) and probabilistic fibre tracking methods (Bucci et al., 2013; Mandelli et al., 2014) provide more accurate tractography results and are less influenced by crossing and kissing fibres compared to deterministic tracking. By contrast, using deterministic algorithms, DTI tract construction can result in artificial fibres which, for example, avoid crossing the superior longitudinal fasciculus. The latter approach, however, still represents the most widely distributed method for presurgical fibre course delineation in the neurosurgical field due to its time efficiency. Aiming at improving the method for clinical purposes, we, therefore, focused our work on deterministic DTI-tractography using a muliple-ROI-approach (Mori and van Zijl, 2002) to compare the use of fMRI versus nTMS (with matched muscles/tasks) as non-invasive functional localizer methods for determination of the cortical M1 seeding ROI.

Given the highly-selected patient collective with surgically removed brain tumours adjacent to M1 and the necessity of complete data sets (including task-fMRI, nTMS, DTI and clear intraoperative DCS results to confirm the eloquent tumour localization), the sample size of 18 patients represents a considerable consecutive set of patients.

4.2. Side effects

No adverse effects were observed related to fMRI or nTMS. This fact confirms the safety data on single pulse nTMS in general (Anand and

Table 2
Course of the nTMS-based in relation to fMRI-based CST fibres (a.-p.). The table provides an overview of the position of CST fibres origination from a cortical nTMS-defined hot-spot as compared to such fibres which were seeding from the fMRI-local activation maxima, with regard to the a.-p. orientation. NTMS-derived CST fibres were classified either rostral, occipital or at the same place compared to the equivalent fMRI-derived fibres (columns). Data were acquired for each somatotopic pair of CST fibres (i.e., fMRI- and nTMS-derived), separately (rows). The table includes both the descriptive statistics for all assessed fibre tracts (numbers printed in black) as well as for the subset of tracts which were classified plausible (numbers printed in grey).

Spatial Position of nTMS–over fMRI–Derived Fibres on Level of Internal Capsule, by Body Part Affiliation			Position of NTMS–Derived CST			Total
			rostral	occipital	at the same place	
M1 Origin	Hand (ABP) contralesional N (%) *(=N plausible)*		7 (39%)	2 (11%)	9 (50%)	18
	Hand (APB) ipsilesional	N (%) [N plausible]	13 (87%) [8]	0 [0]	2 (13%) [2]	15 [10]
	Tongue (LT) ipsilesional	N (%) [N plausible]	4 (40%) [3]	3 (30%) [1]	3 (100%) [3]	10 [7]
	Foot (PM) ipsilesional	N (%) [N plausible]	3 (38%) [2]	2(24%) [1]	3 (38%) [2]	8 [5]
Total ipsilesional		N (%) [N plausible]	20 (61%) [13]	5 (15%) [2]	8 (24%) [7]	33 [22]

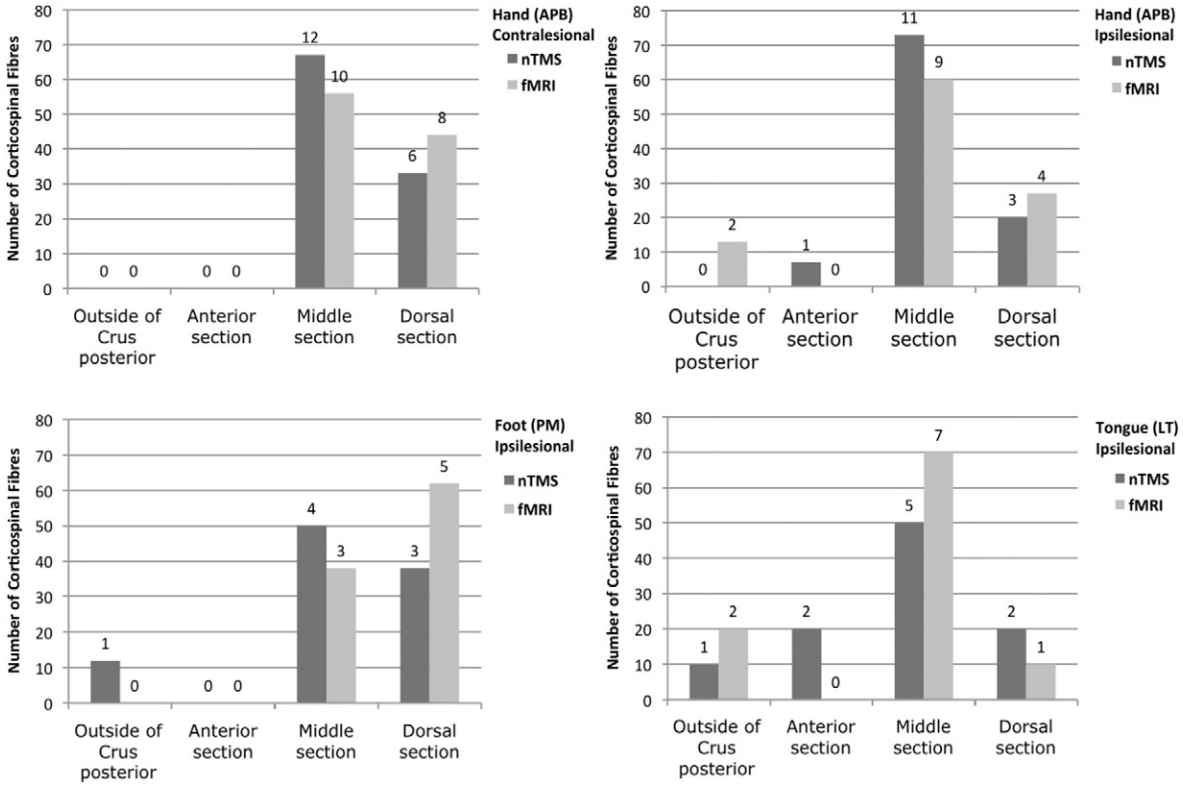

Fig. 6. Course of somatotopic CST fibres within the PLIC. The bar plots display the distribution of the somatotopic CST fibres, originating from the cortical nTMS- (grey), fMRT- (light grey) and DCS- (dark grey) ROIs, within the PLIC. For this analysis, the PLIC was segmented into a central section including the genu (c), a middle (m) and a posterior section (p), according to Fig. 4. The figure includes the percentages of fibres in each segment per total of the respective functional localizer technique (*Y*-axis) as well as the respective count data (numbers above each bar).

Hotson, 2002; Tassinari et al., 2003; Rossi et al., 2009; Tarapore et al., 2016a) and particularly in brain tumour patients (Tarapore et al., 2016b). However, transient headache (<24 h) occurred in 6% of the patients ($N = 2/32$) following nTMS, as expected from previous studies which described this phenomenon as the most frequent side effect associated with TMS (6–60% for repetitive TMS) (Machii et al., 2006).

4.3. Plausibility analysis

4.3.1. General aspects

Algorithms for corticospinal fibre reconstruction, originating from both fMRI- or nTMS-defined seeding ROI volumes, may be biased by inaccurate fibre reconstruction, especially in oedematous areas surrounding the tumour (Min et al., 2013; Lu et al., 2003; Hoefnagels et al., 2014; Jones et al., 2015; Weiss et al., 2015) or regions of crossing fibres (Basser et al., 2000). It is well-known that DTI tracking algorithms are prone to artefacts, especially in areas with an unfavourable signal-to-noise ratio. Therefore, the tractography results can only be regarded as an estimate. Since the tractography algorithm and the DTI data set was identical for the approaches, this potential common systematic bias does, according to the best of our knowledge, not notably affect the comparability of the results. The plausibility analysis was performed by two independent observers and showed good interobserver reliability as previously reported (cf. Weiss et al., 2015).

4.3.2. Comparison of fMRI vs. nTMS as determinants for the cortical seeding ROIs

The plausibility ratings agreed well between fMRI- and nTMS-based tractographies under normal conditions (i.e., on the healthy hemisphere). However, when dealing with cortical seed regions in the tumour surrounding, the use of nTMS as a functional localizer technique led to more plausible results compared to fMRI ($p < 0.05$), especially when comparing hand-related somatotopic fibre tracts. Accordingly, the mean distance between the corresponding somatotopic fibres was greatest at the level of maximal tumour extent where small differences may matter most to the surgeon who aims at maximized but function-preserving tumour resection. Previous studies have investigated the benefits of using fMRI-DTI (Guye et al., 2003; Hendler et al., 2003; Watts et al., 2003; Parmar et al., 2004; Schonberg et al., 2006; Staempfli et al., 2008; Zhu et al., 2012) and, more recently, of using nTMS-DTI (Frey et al., 2012; Krieg et al., 2012; Conti et al., 2014; Weiss et al., 2015) to improve the seed-based tractography of the CST. The better plausibility rates of nTMS-DTI vs. fMRI-DTI in the tumour vicinity which we found in this study may be due to a higher accuracy of nTMS as a functional localizer method for determination of M1 especially in the surrounding of brain tumours (Forster et al., 2011; Coburger et al., 2013; Mangraviti et al., 2013).

4.3.3. Influence of the somatotopic assignment on fibre course plausibility

Somatotopic tractography and anatomical segregation of different ROIs along the course of the CST have been previously addressed by several authors (Park et al., 2008; Yoshiura et al., 2008; Hong et al., 2010b; Kwon et al., 2011; Pan et al., 2012; Conti et al., 2014; Weiss et al., 2015). According to our expectations from considering the unfavourable signal-to-noise effects on the lesional (tumour) hemisphere (Min et al., 2013; Jones et al., 2015) and along with previous findings (Weiss et al., 2015), plausible CSTs reached the highest percentage on the non-affected hemisphere (hand-related fibres) for both nTMS and fMRI. Amongst the different somatotopic nTMS-originated tracts on the tumour side, the hand-related CST fibres showed the most plausible results (93%). Due to anatomical and neurophysiological reasons, the motor representation of the upper limb is known to be best suited for investigation by nTMS and to provide most reliable mapping results (Forster et al., 2012; Weiss et al., 2013; Forster et al., 2014). Therefore,

one may assume that the nTMS motor mapping of the hand representation also provides the most exact determination of the respective M1 core region as compared to the tongue and the foot representation.

In contrast to nTMS, the plausibility rates of fMRI-originated CST fibres did not differ significantly between the somatotopic subsets. This may reflect the fact that the method is less influenced by anatomical factors, e.g. by the location of the foot representation in the relative depth of the interhemispheric fissure, than nTMS.

4.4. Course of the CST

First, the course of the somatotopic CST fibres was described with regard to the distance from the midline. On the level of Monro's foramen, distances were in the range of 23 ± 5 mm (no difference between seeding-ROI techniques or somatotopic affiliation). Those distances, even though not directly comparable due to different levels of measurement, show good overall agreement with the data published by Seo et al. (2012) who described the localization of the CST within the centrum semiovale (leg: 22 ± 2 mm; hand: 26 ± 2 mm).

Secondly, the position of different somatotopic fibres within the PLIC overall agreed well with previous findings and neuroanatomical knowledge: Fibres originating from the non-lesional M1 representation of the hand passed almost exclusively through the dorsal two thirds of the PLIC as previously described by various neuroanatomical (Kretschmann, 1988) and neuroimaging studies (Han et al., 2010) and mostly anteriorly to the foot-related tracts (Lee et al., 2014; Kwon et al., 2014). In contrast, the corticobulbar CST fibres originating from the tongue M1 representation mostly passed through the middle or, at least for nTMS-based tractography results, central segment of the PLIC and hence most anteriorly amongst the somatotopic tracts. In this regard, our results are in line with anatomical knowledge (Cowan and de Vries, 2005) and previous DTI data provided by Jang and Seo (2015). However, the overall, rather variable, distribution of somatotopic tracts within the PLIC of the lesional side in our study certainly reflects tumour-related diffusivity alterations. Thus, this work cannot substitute (and does not aim to replace) anatomical DTI studies under physiological conditions, i.e., in healthy subjects.

Thirdly, we found that, compared to the respective (paired) TMS-fibres, fMRI-derived fibres never passed through the central segment/genu of the PLIC and generally showed a more posterior course. This finding may reflect a certain contribution of somatosensory, thalamocortical fibres to the upper proportion of the fMRI-related tracts (Hong et al., 2010a). A co-activation of the somatosensory cortex in the MRI cannot be excluded although subjects were trained and positioned in a way that touch sensations during the active movement tasks should be avoided. Given the fact that several cases with a significant tumour-induced oedema in the internal capsule were included, the possibility of altered tract continuation in this region of high fibre density and crossings should be considered. This may have led to CST-like fibre tracts originating from the somatosensory cortex but passing through the anterior section of the cerebral peduncles and made it rather impossible to distinguish those fibres from the CST under conditions of tumour-induced alteration of the cortical anatomy.

4.5. Fractional anisotropy

The FA describes the degree of directionality of the diffusion process and therefore serves as a useful indicator for the integrity of reconstructed fibre tracts (Basser and Pierpaoli, 1996, 2011; Chiang et al., 2014; Dacosta-Aguayo et al., 2014; Holtrop et al., 2014; Van der Werff et al., 2014). Accordingly, low FA values are more likely in the presence of tumour-induced oedema (Min et al., 2013; Weiss et al., 2015; Jones et al., 2015). As expected, we observed a significant correlation between the FAT and the fibre course plausibility, regardless of nTMS or fMRI being used to determine the cortical seeding-ROI. The strongest correlation between the FAT and CST plausibility was found for nTMS-based tractography ($p < 0.0001$). Mean FA values of those nTMS-CST, however, did not differ from fMRI-based tracts and were highest for the non-lesional hemisphere but lowest for the face-related somatotopic tracts. These findings may well correspond to the lower agreement between fMRI and nTMS for the determination of the cortical tongue as compared to the hand M1 representation (Weiss et al., 2013). Overall, the diffusion metrics analysis confirmed the FAT to represent a strong indicator for fibre course plausibility as already discussed in our previous work (cf. Weiss et al., 2015). The FA may thus be helpful to assess the risk of erroneous fibre tracking.

4.6. Clinical impact and outlook

Non-invasive preoperative tractography is an excellent novel tool to improve surgical planning and decision-making. This study provides further evidence that the integration of functional localizer techniques such as fMRI or nTMS into the tracking algorithm improves tracking results and points towards nTMS being the better choice for seeding ROI localization in tumour-neighbouring cortical areas.

Over the past decades, diffusion imaging techniques have been constantly improving because of superior gradient hardware, pulse sequences and post-processing algorithms. However, many of these interesting advances including both MRI acquisition and tractography approaches have not yet entered clinical routine. Nonetheless, recent technical innovations such as the use of optimized *b*-values and kurtosis tensor strategies (Marrale et al., 2015; Lanzafame et al., 2016) may further improve the future value of diffusion imaging in routine diagnostics. Furthermore, the improving processor power of modern computers will, in time, enable probabilistic DTI tractography to be fast enough for routine clinical use in preoperative tumour diagnostics.

Despite attempts to further improve tractography strategies, DTI results should always be regarded as approximates and must be re-evaluated intraoperatively, especially when dealing with fast-growing tumours such as high-grade gliomas with considerable tumour-related oedema. In such cases, not only the alterations of diffusivity but also the brain shift after dural opening can be significant. Therefore, non-invasive tractography methods, regardless of their quality, can and should not replace intraoperative confirmation and monitoring by neurophysiological means. Subcortical (monopolar) stimulation represents an excellent tool for intraoperative detection of neighbouring CST fibres (Duffau, 2007; Bello et al., 2008; Kombos et al., 2009; Sanai and Berger, 2010; Szelényi et al., 2011) and even allows rough estimation of the distance between the stimulation site and the respective fibres (Raabe et al., 2014).

However, for precise validation as required for the purposes of this study, technical limitations like the non-linear brain shift after opening the skull were regarded too severe (Romano et al., 2011). In this regard, previous studies have shown a significant intraoperative change of the tumour-to-CST distance at least for contrast-enhancing tumours ranging up to 20 mm (mean 3.9 ± 3.6 mm according to Shahar et al., 2014). Consequently, this study was not designed to measure the accuracy of the tractography results intraoperatively. To answer this additional research question and to further validate DTI tractography results, future studies are required which either use intraoperative MRT/DTI (Nimsky et al., 2005a,b, 2006; Nimsky, 2011; Ostrý et al., 2013; Shahar et al., 2014) or avoid the brain shift by means of stereotactic approaches (Forster et al., 2015).

In addition to subcortical stimulation, awake surgery represents a versatile method to monitor not only integrity of basic functional structures such as the corticospinal pathway but also complex functional networks such as speech or other neurocognitive functions (Duffau et al., 2003; Pereira et al., 2009; De Benedictis et al., 2010; De Witt Hamer et al., 2012; Shinoura et al., 2013; Surbeck et al., 2015). Awake surgery can generally be regarded as a well tolerable (Beez et al., 2013) and highly robust method. Therefore, the combination of pre- and intraoperative cortical and subcortical mapping techniques with awake surgery

should be considered the ideal approach regarding function-preserving surgery of eloquent brain tumours today (Duffau et al., 2003, 2005; Kombos and Suess, 2009; Freyschlag and Duffau, 2014).

5. Conclusions

The study provides further evidence that deterministic CST tractography using a multiple-ROI approach with a seeding ROI on the cortical level defined by fMRI or nTMS and an additional cubic ROI in the area of the anterior inferior pons is a feasible approach for presurgical delineation of the pyramidal tract in brain tumour patients. Comparing the two functional localizer techniques, nTMS seems to provide more plausible tractography results for the lesional hemisphere. Depending on the somatotopic assignment of the fibre tracts, nTMS- and fMRI-related tracts usually differed by few millimeters with the nTMS-originated fibres following a more rostral course as compared to the according fMRI-based tracts. In line with our previous work, the FA values correlated strongly with plausibility rates in all functional localizer groups but most for the nTMS-based tracts. Despite all progress regarding further standardisation and improvement of non-invasive tractography, the limitations of the methods such as particularly the unfavourable signal-to-noise ratio in the area of tumour-induced oedema and fibre crossings should always be kept in mind and tractography results should thus be regarded as estimates. The current state-of-the-art regarding surgical removal of brain tumours in the neighbourhood of the CST should therefore not be based on non-invasive techniques alone but explicitly include direct subcortical stimulation and/or awake surgery. Intraoperative MRI may further complement these methods and can serve to validate the tractography techniques along with stereotactic approaches.

Supplementary data to this article can be found online at http://dx.doi.org/10.1016/j.nicl.2016.11.022.

Grants and fundings

We thank the German Research Foundation (DFG) for funding of the nTMS machine (Nexstim NBS 4.2; grant: INST 1856/50-1). The first author (CWL) received additional funding by the Faculty of Medicine of the University of Cologne (grant: Gerok 8/2016).

References

Ahdab, R., Ayache, S.S., Brugières, P., et al., 2016. The hand motor hotspot is not always located in the hand knob: a neuronavigated transcranial magnetic stimulation study. Brain Topogr. 29 (4), 590–597.
Anand, S., Hotson, J., 2002. Transcranial magnetic stimulation: neurophysiological applications and safety. Brain Cogn. 50, 366–386.
Auriat, A.M., Borich, M.R., Snow, N.J., et al., 2015. Comparing a diffusion tensor and non-tensor approach to white matter fiber tractography in chronic stroke. Neuroimage Clin. 7, 771–781.
Barone, D.G., Lawrie, T.A., Hart, M.G., 2014. Image guided surgery for the resection of brain tumours. Cochrane Database Syst. Rev. 1.
Basser, P.J., Pierpaoli, C., 1996. Microstructural and physiological features of tissues elucidated by quantitative-diffusion-tensor MRI. J. Magn. Res. B 111, 209–219.
Basser, P.J., Pierpaoli, C., 2011. Recollections about our 1996 JMR paper on diffusion anisotropy. J. Magn. Res. 213, 571–572.
Basser, P.J., Pajevic, S., Pierpaoli, C., et al., 2000. In vivo fiber tractography using DTI-MRI data. Magn. Reson. Med. 44 (4), 625–632.
Beez, T., Boge, K., Wager, M., et al., 2013. Tolerance of awake surgery for glioma: a prospective European Low Grade Glioma Network multicenter study. Acta Neurochir. 155, 1301–1308.
Bello, L., Gambini, A., Castellano, A., et al., 2008. Motor and language DTI Fiber Tracking combined with intraoperativ subcortical mapping for surgical removal of gliomas. NIMG 39, 369–382.
Benjamini, Y., Hochberg, Y., 1995. Controlling the false discovery rate: a practical and powerful approach to multiple testing. J. R. Stat. Soc. Ser. B 57, 289–300.
Bucci, M., Mandelli, M.L., Berman, J.I., et al., 2013. Quantifying diffusion MRI tractography of the corticospinal tract in brain tumors with deterministic and probabilistic methods. NeuroImage Clin. 3, 361–368.
Chiang, C.W., Wang, Y., Sun, P., et al., 2014. Quantifying white matter tract diffusion parameters in the presence of increased extra-fiber cellularity and vasogenic edema. NeuroImage 101, 310–319.
Coburger, J., Musahl, C., Henkes, H., et al., 2013. Comparison of navigated transcranial magnetic stimulation and functional magnetic resonance imaging for preoperative mapping in rolandic tumor surgery. Neurosurg. Rev. 36 (1), 65–76.
Conti, A., Raffa, G., Granata, F., et al., 2014. Navigated transcranial magnetic stimulation for "somatotopic" tractography of the corticospinal tract. Oper. Neurosurg. 10, 542–554.
Conturo, T.E., Lori, N.F., Cull, T.S., et al., 1999. Tracking neuronal fiber pathways in the living human brain. Proc. Natl. Acad. Sci. U. S. A. 96 (18), 10422–10427.
Cowan, F.M., de Vries, L.S., 2005. The internal capsule in neonatal imaging. Semin. Fetal Neonatal Med. 10, 461–474.
Dacosta-Aguayo, R., Grana, M., Fernández-Andújar, M., et al., 2014. Structural integrity of the contralesional hemisphere predicts cognitive impairment in ischemic stroke at three months. PLoS One 9 (1), e86119.
De Benedictis, A., Moritz-Gasser, S., Duffau, H., 2010. Awake mapping optimizes the extent of resection of low-grade gliomas in eloquent areas. Neurosugery 66, 1074–1084.
De Witt Hamer, P.C., Robles, S.G., Zwinderman, A.H., et al., 2012. Impact of intraoperative stimulation brain mapping on glioma surgery outcome: a meta-analysis. J. Clin. Oncol. 30, 2559–2565.
Diekhoff, S., Uludag, K., Sparing, R., et al., 2011. Functional localization in the human brain: Gradient-Echo, Spin-Echo, and arterial spin-labeling fMRI compared with neuronavigated TMS. Hum. Brain Mapp. 32 (3), 341–357.
Duffau, H., 2007. Contribution of cortical and subcortical electrostimulation in brain glioma surgery: methodological and functional considerations. Clin. Neurophysiol. 37, 373–382.
Duffau, H., Capelle, L., Denvil, D., et al., 2003. Usefulness of intraoperative electrical subcortical mapping during surgery for low-grade gliomas located within eloquent brain regions: functional results in a consecutive series of 103 patients. J. Neurosurg. 98, 764–778.
Duffau, H., Lopes, M., Arthuis, F., et al., 2005. Contribution of intraoperative electrical stimulations in surgery of low grade gliomas: a comparative study between two series without (1985–96) and with (1996–2003) functional mapping in the same institution. J. Neurol. Neurosurg. Psychiatry 76, 845–851.
Forster, M.T., Hattingen, E., Senft, C., Gasser, T., Seifert, V., Szelényi, A., 2011. Navigated transcranial magnetic stimulation and functional magnetic resonance imaging: advanced adjuncts in preoperative planning for central region tumors. Neurosurg. 68 (5), 1317–1324.
Forster, M.T., Senft, C., Hattingen, E., et al., 2012. Motor cortex evaluation by nTMS after surgery of central region tumors: a feasibility study. Acta Neurochir. 154, 1351–1359.
Forster, M.T., Limbart, M., Seifert, V., Senft, C., 2014. Test-retest reliability of navigated transcranial magnetic stimulation of the motor cortex. Neurosurgery 10 (Suppl. 1), 51–55.
Forster, M.T., Hoecker, A.C., Kang, J.S., et al., 2015. Does navigated transcranial magnetic stimulation increase the accuracy of tractography? A prospective clinical trial based on intraoperative motor evoked potential monitoring during deep brain stimulation. Neurosurgery 76 (6), 766–776.
Frey, D., Strack, V., Wiener, D., et al., 2012. A new approach for corticospinal tract reconstruction based on navigated transcranial stimulation and standardized fractional anisotropy values. NeuroImage 62, 1600–1609.
Freyschlag, C.F., Duffau, H., 2014. Awake brain mapping of cortex and subcortical pathways in brain tumor surgery. J. Neurosurg. Sci. 58 (4), 199–213.
Gaetz, W., Scantlebury, N., Widjaja, E., et al., 2010. Mapping of the cortical spinal tracts using magnetoencephalography and diffusion tensor tractography in pediatric brain tumor patients. Childs Nerv. Syst. 26, 1639–1645.
Glickman, M.E., Rao, S.R., Schultz, M.R., 2014. False discovery rate control is a recommended alternative to Bonferroni-type adjustments in health studies. J. Clin. Epidemiol. 67, 850–857.
Gustard, S., Fadili, J., Williams, E.J., Hall, L.D., Carpenter, T.A., Brett, M., Bullmore, E.T., 2001. Effect of slice orientation on reproducibility of fMRI motor activation at 3 Tesla. Magn. Reson. Imaging. 19 (10), 1323–1331.
Guye, M., Parker, G.J.M., Symms, M., et al., 2003. Combined functional MRI and tractography to demonstrate the connectivity of the human primary motor cortex in vivo. NeuroImage 19, 1349–1360.
Han, B.S., Hong, J.H., Hong, C., et al., 2010. Location of the corticospinal tract at the corona radiate in human brain. Brain Res. 1326, 75–80.
Hendler, T., Pianka, P., Sigal, M., et al., 2003. Delineating gray and white matter involvement in brain lesions: three-dimensional alignment of functional magnetic resonance and diffusion-tensor imaging. J. Neurosurg. 99 (6), 1018–1027.
Hoefnagels, F.W.A., De Witt, H.P., Sanz-Arigita, E., et al., 2014. Differentiation of edema and glioma infiltration: proposal of a DTI-based probability map. J. Neuro-Oncol. 120 (1), 187–198.
Holtrop, J.L., Loucks, T.M., Sosnoff, J.J., Sutton, B.P., 2014. Investigating age-related changes in fine motor control across different effectors and the impact of white matter integrity. NeuroImage 96, 81–87.
Hong, J.H., Son, S.M., Jang, S.H., 2010a. Identification of spinothalamic tract and its related thalamocortical fibers in human brain. Neurosci. Lett. 468, 102–105.
Hong, J.H., Son, S.M., Jang, S.H., 2010b. Somatotopic location of corticospinal tract at pons in human brain: a diffusion tensor tractography study. NeuroImage 51, 952–955.
Ilmoniemi, R.J., Ruohonen, J., Karhu, J., 1999. Transcranial magnetic stimulation—a new tool for functional imaging of the brain. Crit. Rev. Biomed. Eng. 27 (3–5), 241–284.
Jang, S.H., Seo, J.P., 2015. The anatomical location of the corticobulbar tract at the corona radiata in the human brain: diffusion tensor tractography study. Neurosci. Lett. 590, 80–83.
Janssen, A.M., Oostendorp, T.F., Stegeman, D.F., 2015. The coil orientation dependency of the electrical field induced by TMS for M1 and other brain areas. J. Neuroeng. Rehabil. 17, 12–47.

Jones, T.L., Bymes, T.J., Yang, G., et al., 2015. Brain tumor classification using the diffusion tensor image segmentation (D-SEG) technique. Neuro-Oncology 17 (3), 466–476.
Julkunen, P., Saisanen, L., Danner, N., et al., 2009. Comparison of navigated and non-navigated transcranial magnetic stimulation for motor cortex mapping, motor threshold and motor evoked potentials. NeuroImage 44 (3), 790–795.
Karnofsky, D.A., Burchenal, J.H., 1949. The clinical evaluation of chemotherapeutic agents in cancer. In: MacLeod, C.M. (Ed.), Evaluation of Chemotherapeutic Agents. Columbia University Press, New York, p. 196.
Kombos, T., Suess, O., 2009. Neurophysiological basis of direct cortical stimulation and applied neuroanatomy of the motor cortex: a review. Neurosurg. Focus. 27 (4), E3.
Kombos, T., Suess, O., Vajkoczy, P., 2009. Subcortical mapping and monitoring during insular tumor surgery. Neurosurg. Focus. 27 (4), E5.
Kretschmann, H.J., 1988. Location of the corticospinal fibres in the internal capsule in man. J. Anat. 160, 219–225.
Krieg, S.M., Buchmann, N.H., Gempt, J., et al., 2012. Diffusion tensor imaging fiber tracking using navigated brain stimulation-a feasibility study. Acta Neurochir. 154, 555–563.
Kwon, H.G., Hong, J.H., Jang, S.H., 2011. Anatomic location and somatotopic arrangement of the corticospinal tract at the cerebral peduncle in the human brain. AJNR Am. J. Neuroradiol. 32, 2116–2119.
Kwon, H.G., Yang, J.H., Park, J.B., et al., 2014. Anatomical location and somatotopic organization of the corticospinal tract in the corona radiata of the normal human brain: a diffusion tensor tractography study. Neuroreport 25, 710–714.
Lanzafame, S., Giannelli, M., Garaci, F., et al., 2016. Differences in Gaussian diffusion tensor imaging and non-Gaussian diffusion kurtosis imaging model-based estimates of diffusion tensor invariants in the human brain. Med. Phys. 43 (5), 2464.
Le Bihan, D., Mangin, J.F., Poupon, C., et al., 2001. Diffusion tensor imaging: concepts and application. J. Magn. Reson. Imaging 13 (4), 534–546.
Lee, D.H., Hong, C., Han, B.S., 2014. Diffusion-tensor magnetic resonance imaging for hand and foot fibers location at the corona radiata: comparison with two lesion studies. Front. Hum. Neurosci. 8, 752.
Lehéricy, S., Duffau, H., Cornu, P., et al., 2000. Correspondence between functional magnetic resonance imaging somatotopy and individual brain anatomy of the central region: comparison with intraoperative stimulation in patients with brain tumors. J. Neurosurg. 92, 589–598.
Lu, S., Ahn, D., Johnson, G., Cha, S., 2003. Peritumoral diffusion tensor imaging of high-grade gliomas and metastatic brain tumors. AJNR Am. J. Neuroradiol. 24, 937–941.
Machii, K., Cohen, D., Ramos-Estebanez, C., Pascual-Leone, A., 2006. Safety of rTMS to non-motor cortical areas in healthy participants and patients. Clin. Neurophysiol. 117, 455–471.
Mandelli, M.L., Berger, M.S., Bucci, M., et al., 2014. Quantifying accuracy and precision of diffusion MR tractography of the corticospinal tract in brain tumors. J. Neurosurg. 121 (2), 349–358.
Mangraviti, A., Casali, C., Cordella, R., et al., 2013. Practical assessment of preoperative functional mapping techniques: navigated transcranial magnetic stimulation and functional magnetic resonance imaging. Neurol. Sci. 34 (9), 1551–1557.
Marrale, M., Collura, G., Brai, M., et al., 2015. Physics, techniques and review of neuroradiological applications of diffusion kurtosis imaging (DKI). Clin. Neuroradiol. Epub ahead of print. 10.1007/s00062-015-0469-9.
McNemar, Q., 1947. Note on the sampling error of the difference between correlated proportions or percentages. Psychometrika 12 (2), 153–157.
Min, Z.G., Niu, C., Rana, N., et al., 2013. Differentiation of pure vasogenic edema and tumor-infiltrated edema in patients with peritumoral edema by analyzing the relationship of axial and radial diffusivities on 3.0T MRI. Clin. Neurol. Neurosurg. 115 (8), 1366–1370.
Mori, S., van Zijl, P.C.M., 2002. Fiber tracking: principles and strategies–a technical review. NMR Biomed. 15, 468–480.
Mori, S., Kaufmann, W.E., Davatzikos, C., et al., 2002. Imaging cortical association tracts in the human brain using diffusion-tensor-based axonal tracking. Magn. Reson. Med. 47 (2), 215–223.
Nimsky, C., 2011. Intraoperative acquisition of fMRI and DTI. Neurosurg. Clin. N. Am. 22 (2), 269–277.
Nimsky, C., Ganslandt, O., Hastreiter, P., et al., 2004. Intraoperative diffusion-tensor MR imaging: shifting of white matter tracts during neurosurgical procedures – initial experience. Radiology 234 (1), 218–225.
Nimsky, C., Ganslandt, O., Hastreiter, P., et al., 2005a. Intraoperative diffusion-tensor MR imaging: shifting of white matter tracts during neurosurgical procedures – initial experience. Radiology 234, 218–225.
Nimsky, C., Ganslandt, O., Hastreiter, P., et al., 2005b. Preoperative and intraoperative diffusion tensor imaging-based fiber tracking in glioma surgery. Neurosurgery 65, 130–138.
Nimsky, C., Ganslandt, O., Merhof, D., et al., 2006. Intraoperative visualization of the pyramidal tract by diffusion-tensor-imaging-based fiber tracking. NeuroImage 30 (4), 1219–1229.
Nimsky, C., Ganslandt, O., Hastreiter, P., Wang, R., Sorensen, A.G., Fahlbusch, R., 2007. Preoperative and intraoperative diffusion tensor imaging-based fiber tracking in glioma surgery. Neurosurgery 61 (1 Suppl), 178–185.
Ohue, S., Kohno, S., Inoue, A., et al., 2012. Accuracy of diffusion tensor magnetic resonance imaging-based tractography for surgery of gliomas near the pyramidal tract: a significant correlation between subcortical electrical stimulation and postoperative tractography. Neurosurgery 70, 283–294.
Ostrý, S., Belsan, T., Otáhal, J., et al., 2013. Is intraoperative diffusion tensor imaging at 3.0T comparable to subcortical corticospinal tract mapping? Neurosurgery 73, 797–807.
Pan, C., Peck, K.K., Young, R.J., Holodny, A.I., 2012. Somatotopic organization of motor pathways in the internal capsule: a probabilistic diffusion tractography study. AJNR Am. J. Neuroradiol. 33, 1274–1280.
Park, J.K., Kim, B.S., Kim, S.H., et al., 2008. Evaluation of the somatotopic organization of corticospinal tracts in the internal capsule and cerebral peduncle: results of diffusion-tensor MR tractography. Korean J. Radiol. 9, 191–195.
Parmar, H., Sitoh, Y.Y., Yeo, T.T., 2004. Combined magnetic resonance tractography and functional magnetic resonance imaging in evaluation of brain tumors involving the motor system. J. Comput. Assist. Tomogr. 28 (4), 551–556.
Penfield, W., Rasmussen, T., 1950. The Cerebral Cortex of Man. A Clinical Study of Localization of Function. The Macmilian Comp, New York.
Pereira, L.C.M., Oliveira, K.M., L'Abbate, G.L., et al., 2009. Outcome of fully awake craniotomy for lesions near the eloquent cortex: analysis of a prospective surgical series of 79 supratentorial primary brain tumors with long follow-up. Acta Neurochir. 151, 1215–1230.
Petrides, M., Pandya, D.N., 1984. Projections to the frontal cortex from the posterior parietal region in the rhesus monkey. J. Comp. Neurol. 228, 105–116.
Prabhu, S.S., Gasco, J., Tummala, S., et al., 2011. Intraoperative magnetic resonance imaging-guided tractography with integrated monopolar subcortical functional mapping for resection of brain tumors. J. Neurosurg. 114, 719–726.
Qazi, A.A., Radmanesh, A., O'Donnell, L., et al., 2009. Resolving crossings in the corticospinal tract by two-tensor streamline tractography: method and clinical assessment using fMRI. NeuroImage 47 (Suppl. 2), T98–106.
Raabe, A., Beck, J., Schucht, P., Seidel, K., 2014. Continuous dynamic mapping of the corticospinal tract during surgery of motor eloquent brain tumors: evaluation of a new method. J. Neurosurg. 120 (5), 1015–1024.
Raffin, E., Pellegrino, G., Di Lazzaro, V., et al., 2015. Bringing transcranial mapping into shape: sulcus-aligned mapping captures motor somatotopy in human primary motor hand area. NeuroImage 120, 164–175.
Rödel, R.M., Laskawi, R., Markus, H., Neupert, P., 1999. Possible one-dimensional determination of cortical representative fields of mimetic lower lip muscles by transcranial magnetic stimulation. [Article in German]. Laryngorhinootologie 78 (10), 552–556.
Rödel, R.M., Laskawi, R., Markus, H., 2001. Cortical representation of the orbicularis oculi muscle as assessed by transcranial magnetic stimulation (TMS). Laryngoscope 111, 2005–2011.
Rödel, R.M., Laskawi, R., Markus, H., 2003. Tongue representation in the lateral cortical motor region of the human brain as assessed by transcranial magnetic stimulation. Ann. Otol. Rhinol. Laryngol. 112 (1), 71–76.
Romano, A., D'Andrea, G., Calabria, L.F., et al., 2011. Pre- and intraoperative Tractographic evaluation of corticospinal tract shift. Neurosurgery 69, 696–705.
Rossi, S., Hallett, M., Rossini, P.M., et al., 2009. Safety, ethical considerations, and application guidelines for the use of transcranial magnetic stimulation in clinical practice and research. Clin. Neurophysiol. 120 (12), 2008–2039.
Rossini, P.M., Barker, A.T., Berardelli, A., et al., 1994. Non-invasive electrical and magnetic stimultion of the brain, spinal cord and roots: basic principles and procedures for routine clinical application. Report of an IFCN committee. Electroencephalogr. Clin. Neurophysiol. 91 (2), 79–92.
Ruohonen, J., Karhu, J., 2010. Navigated transcranial magnetic stimulation. Clin. Neurophysiol. 40, 7–17.
Saisanen, L., Julkunen, P., Niskanen, E., et al., 2008. Motor potentials evoked by navigated transcranial magnetic stimulation in healthy subjects. J. Clin. Neurophysiol. 25 (6), 420–428.
Salinas, F.S., Lancaster, J.L., Fox, P.T., 2007. Detailed 3D models of the induced electric field of transcranial magnetic stimulation coils. Phys. Med. Biol. 52, 2879–2892.
Sanai, N., Berger, M.S., 2010. Intraoperative stimulation techniques for functional pathway preservation and glioma resection. Neurosurg. Focus. 28 (2), E1.
Scheufler, K.M., Zentner, J., 2002. Total intravenous anesthesia for intraoperative monitoring of the motor pathways: an integral view combining clinical and experimental data. J. Neurosurg. 96 (3), 571–579.
Schonberg, T., Pianka, P., Hendler, T., et al., 2006. Characterization of displaced white matter by brain tumors using combined DTI and fMRI. NeuroImage 30 (4), 1100–1111.
Seo, J.P., Chang, P.H., Jang, S.H., 2012. Anatomical location of the corticospinal tract according to somatotopies in the centrum semiovale. Neurosci. Lett. 523 (2), 111–114.
Seo, J.P., Jang, S.H., 2013. Characteristics of corticospinal tract area according to Pontine level. Yonsei Med. J. 54 (3), 785–787.
Shahar, T., Rozovski, U., Marko, N.F., et al., 2014. Preoperative imaging to predict intraoperative changes in tumor-to-corticospinal tract distance: an analysis of 45 cases using high-field intraoperative magnetic resonance imaging. Neurosurgery 75 (1), 23–30.
Shinoura, N., Midorikawa, A., Yamada, R., et al., 2013. Awake craniotomy for brain lesions within and near the primary motor area: a retrospective analysis of factors associated with worsened paresis in 102 consecutive patients. Surg. Neurol. Int. 4, 149.
Staempfli, P., Reischauer, C., Jaermann, T., et al., 2008. Combining fMRI and DTI: a framework for exploring the limits of fMRI-guided DTI fiber tracking and for verifying DTI-based fiber tractography results. NeuroImage 39, 119–126.
Strick, P.L., Preston, J.B., 1983. Input-output organization of the primate motor cortex. Adv. Neurol. 39, 321–327.
Surbeck, W., Hildebrandt, G., Duffau, H., 2015. The evolution of brain surgery on awake patients. Acta Neurochir. 157 (1), 77–84.
Svolos, P., Kousi, E., Kapsalaki, E., et al., 2014. The role of diffusion and perfusion weighted imaging in the differential diagnosis of cerebral tumors: a review and future perspectives. Cancer Imaging 14, 20.
Szelényi, A., Senft, C., Jardan, M., et al., 2011. Intra-operative subcortical electrical stimulation: a comparison of two methods. Clin. Neurophysiol. 122, 1470–1475.
Tarapore, P.E., Picht, T., Bulubas, L., et al., 2016a. Safety and tolerability of navigated TMS in healthy volunteers. Clin. Neurophysiol. 127 (3), 1916–1918.
Tarapore, P.E., Picht, T., Bulubas, L., et al., 2016b. Safety and tolerability of navigated TMS for preoperative mapping in neurosurgical patients. Clin. Neurophysiol. 127 (3), 1895–1900.

Tassinari, C.A., Cincotta, M., Zaccara, G., Michelucci, R., 2003. Transcranial magnetic stimulation and epilepsy. Clin. Neurophysiol. 114, 777–798.
Van der Werff, S.J.A., Andela, C.D., Pannekoek, J.N., et al., 2014. Widespread reductions of white matter integrity in patients with long-term remission of Cushing's disease. NeuroImage Clin. 4, 659–667.
Vassal, F., Schneider, F., Nuti, C., 2013. Intraoperative use of diffusion tensor imaging-based tractography for resection of gliomas located near the pyramidal tract: comparison with subcortical stimulation mapping and contribution to surgical outcomes. Br. J. Neurosurg. 27 (5), 668–675.
Verstynen, T., Jarbo, K., Pathak, S., Schneider, W., 2011. In vivo mapping of microstructural Somatotopies in the human corticospinal pathways. J. Neurophysiol. 105, 336–346.
Watts, R., Liston, C., Niogi, S., Ulug, A.M., 2003. Fiber tracking using magnetic resonance diffusion tensor imaging and its applications to human brain development. Ment. Retard. Dev. Disabil. Res. Rev. 9 (3), 168–177.
Wehner, T., 2013. The role of functional imaging in the tumor patient. Epilepsia 54 (Suppl. 9), 44–49.
Weiss, C., Nettekoven, C.M., Rehme, A., et al., 2012. The importance of latency correction for navigated TMS mapping, especially of the face and the tongue area: a technical note. Klin. Neurophysiol. 43, P137.
Weiss, C., Nettekoven, C., Rehme, A.K., et al., 2013. Mapping the hand, foot and face representations in the primary motor cortex — retest reliability of neuronavigated TMS versus functional MRI. NeuroImage 66, 531–542.
Weiss, C., Tursunova, I., Neuschmelting, V., et al., 2015. Improved nTMS- and DTI-derived CST tractography through anatomical ROI seeding on anterior pontine level compared to the internal capsule. Neuroimage Clin. 20 (7), 424–437.
Wengenroth, M., Blatow, M., Guenther, J., et al., 2011. Diagnostic benefits of presurgical fMRI in patients with brain tumors in the primary sensorimotor cortex. Eur. Radiol. 21, 1517–1525.
Wu, J.S., Zhou, L.F., Tang, W.J., et al., 2007. Clinical evaluation and follow-up outcome of diffusion tensor imaging-based functional neuronavigation: a prospective, controlled study in patients with gliomas involving pyramidal tracts. Neurosurgery 61 (5), 935–948.
Yoshiura, T., Kumazawa, S., Noguchi, T., et al., 2008. MR tractography based on directional diffusion function: validation in somatotopic organization of the pyramidal tract. Acad. Radiol. 15 (2), 186–192.
Yousry, T.A., Schmid, U.D., Alkadhi, H., et al., 1997. Localization of the motor hand area to a knob on the precentral gyrus. A new landmark. Brain 120 (1), 141–157.
Zhu, F.P., Wu, J.S., Song, Y.Y., et al., 2012. Clinical application of motor pathway mapping using diffusion tensor imaging tractography and intraoperative direct subcortical stimulation in cerebral glioma surgery: a prospective cohort study. Neurosurgery 71, 1170–1184.
Zilles, K., Schleicher, A., Langemann, C., et al., 1997. Quantitative analysis of sulci in the human cerebral cortex: development, regional heterogeneity, gender difference, asymmetry, intersubject variability and cortical architecture. Hum. Brain Mapp. 5, 218–221.
Zolal, A., Hejci, A., Malucelli, A., et al., 2013. Distant white-matter diffusion changes caused by tumor growth. J. Neuroradiol. 40 (2), 71–80.